

Studies on anode mass composition and cathode flow field design for small-scale to large-scale direct methanol fuel cell stack systems

Cite as: AIP Advances 12, 125316 (2022); <https://doi.org/10.1063/5.0121729>

Submitted: 24 August 2022 • Accepted: 05 December 2022 • Published Online: 21 December 2022

 Thanarajan Kumaresan,  Karthikeyan Palaniswamy,  Ashley Fly, et al.



View Online



Export Citation



CrossMark

ARTICLES YOU MAY BE INTERESTED IN

[Ultrafast silicon threshold circuitry for chaotic laser time series](#)

AIP Advances 12, 125225 (2022); <https://doi.org/10.1063/5.0127470>



Studies on anode mass composition and cathode flow field design for small-scale to large-scale direct methanol fuel cell stack systems

Cite as: AIP Advances 12, 125316 (2022); doi: 10.1063/5.0121729

Submitted: 24 August 2022 • Accepted: 5 December 2022 •

Published Online: 21 December 2022



View Online



Export Citation



CrossMark

Thanarajan Kumaresan,¹  Karthikeyan Palaniswamy,^{1,a)}  Ashley Fly,²  and Senthilarasu Sundaram³ 

AFFILIATIONS

¹Fuel Cells and Energy Systems Laboratory, Department of Automobile Engineering, PSG College of Technology, Coimbatore 641004, India

²Department of Aeronautical and Automotive Engineering, Loughborough University, Loughborough LE11 3TT, United Kingdom

³Cybersecurity and Systems Engineering, School of Computing, Engineering and the Built Environment, Edinburgh Napier University, Merchiston Campus, Edinburgh EH10 5DT, United Kingdom

^{a)}Author to whom correspondence should be addressed: apk.auto@psgtech.ac.in

ABSTRACT

In this research, the performance studies of a single cell Direct Methanol Fuel Cell with three different mass compositions (20%, 40%, and 60%) of platinum at anode infused in NiTiO₃/C and multiple cathode flow fields, such as serpentine, parallel, and sinuous, with 25 cm² active area. 40% platinum mass composition has been reported with a maximum power density of 24.42 mW/cm², which is 26.8% and 10.4% higher than the performance observed in 20% and 60% platinum mass composition, respectively, on serpentine flow field. Among the various cathode flow fields, sinuous flow field provided the maximum power density of 28.69 mW/cm², which is 17.48% and 53.83% higher in performance than that of serpentine and parallel flow fields, respectively. The best-performing catalyst mass composition and flow field, viz., 40% mass composition and sinuous flow field are scaled up to a 100 cm² active area, and the results showed 16% lower performance compared to a 25 cm² active area. A three-cell stack is fabricated with the best performing combination with the 100 cm² active area that delivered a peak power output of 5.8 W, which resulted in 19.4% lower performance than 100 cm². The stack was tested for stability for 48 h at constant voltage mode and was found that 0.002 W deviation for the entire period.

© 2022 Author(s). All article content, except where otherwise noted, is licensed under a Creative Commons Attribution (CC BY) license (<http://creativecommons.org/licenses/by/4.0/>). <https://doi.org/10.1063/5.0121729>

I. INTRODUCTION

The constant increase in energy consumption and the need to lower the greenhouse gas emissions have fueled the hunt for alternative energy sources.¹ Many experts and academics rely on Fuel Cell (FC) technology to meet the growing needs of green energy. Hence, FCs are considered to be the most effective, silent, and clean energy technologies.^{2,3} FC converts chemical energy to electrical energy directly, thereby eliminating the need for fuel combustion making it more efficient.⁴

Since Direct Methanol Fuel Cell (DMFC) has better energy density, as well as it does not require a fuel reformer, and can operate at lower temperatures than other fuel cell technologies, it is

the most promising and efficient energy conversion device for low power applications.⁵ DMFCs can be used for applications, such as mobile chargers, forklifts, and boats.^{6,7} Although DMFC pose a lot of advantages, it also has some drawbacks, such as slow reaction rate at the anode, methanol fuel crossover through the membrane, and the usage of high platinum loading as electro-catalysts hindering commercialization.^{8,9}

To minimize the system's cost, reducing the loading of noble catalysts by increasing their effective utilization is attempted in this work.¹⁰ To reduce the usage of noble metals and to enhance the catalytic activity, many researchers introduced metal oxides as the supportive material with noble metals.^{11–13} Material scientists proved the integration of certain metal oxides as an active

support material for anode electrocatalyst in DMFCs to improve cell performance. Ercelik *et al.*¹³ studied the performance of different weight ratios (5, 15, and 25 wt. %) of TiO₂ as anode co-catalyst with respect to commercial catalysts. The experimental results showed that 5 wt. % delivered a maximum performance of 709.32 W/m² at 80 °C and 1M methanol concentration. 5 wt. % TiO₂ was found more stable as anode catalyst of DMFC and exhibited improved electrochemical activity and complete usage of platinum available on the catalyst layer. Shan *et al.*¹⁴ investigated the particle size of IrO₂ in Pt–NT toward the performance improvement of DMFC and reported that the performance and electrochemical activity of DMFC was highly influenced by the particle size. The particle size of Pt (2.9–5.5 nm) and IrO₂ (4.5–11.3 nm) delivered better performance, which is comparable to commercial catalysts. Scibioh *et al.*¹⁵ developed a metal oxide catalyst (Pt–CeO₂/C) to replace the commercial catalyst (Pt–Ru/C). The composition of CeO₂ was varied from 3% to 12%, and Pt was fixed as 40%. From their experimental results, 40% Pt with 9% CeO₂ exhibited enhanced catalytic activity and stability than commercial catalysts. The Pt–CeO₂/C composition was more promising and less expensive for methanol oxidation reaction (MOR) due to its bifunctional and intrinsic mechanism. Maiyalagan and Khan¹⁶ studied the effect of V₂O₅ metal oxide as the co-catalyst for MOR. Pt–V₂O₅/C showed higher catalytic activity and stability, which could be attributed to the combined effect between Pt and V₂O₅ to avoid the electrode poison. The catalyst material delivered a maximum current density of 17.4 mA/cm², which is 42% higher than commercial catalyst (Pt/C). This was attributed to the conversion of CO to CO₂ at lower potential. The oxygen species available on the surface of V₂O₅ supported the oxidation of CO intermediates to CO₂ and released the Pt sites for further chemical reaction. Justin and Ranga Rao¹¹ studied the incorporation of MoO₃ on Pt/C to improve MOR activity. The solid synergy between Pt and MoO₃ promotes the electrocatalytic activity and stability for MOR. In acid solution, the nonconducting MoO₃ was reduced electrochemically to improve conductivity by hydrogen molybdenum bronze (H_xMoO₃) and delivered 128% higher current density than Pt–Ru/C. The hydrogen molybdenum bronze supported the conversion of CO to CO₂ to maintain the activity and ability of the electrode surface to oxidize methanol. From various metal oxides, TiO₂ has been identified as a promising MOR reaction promoter with good stability. The metal oxide weakens the Pt–CO bond that improves CO removal from Pt surfaces.¹⁷ TiO₂ enhances OH adsorption and the conversion of toxic CO to CO₂ during the MOR process. However, a high electrically conductive material is required to collect and transfer the electrons effectively because TiO₂ has low electric conductivity. To overcome that problem, a higher amount of platinum was loaded on TiO₂¹⁸ along with an electric conductivity material, such as carbon,^{19–21} Np doping,^{18,22,23} and modifying the stoichiometry.²⁴ Thiagarajan *et al.*²⁵ found that Pt–NiTiO₃/C has better polarization and maintains a stable current than Pt/C. The combined effect of Pt and NiTiO₃ allows NiTiO₃ to accelerate CO_{ads} oxidation. The performance of NiTiO₃ was experimentally proved with a 5 cm² active area and compared with commercial catalysts of DMFC.²⁶ Wie *et al.*²⁷ investigated the impact of catalyst composition on the performance of DMFC. Increased Pt loading resulted in the reduction of Pt utilization, which indicates excess Pt was available in the catalyst layer. As a result, optimizing the mass

composition of catalyst materials is required to improve DMFC performance.

For best performance, low operating cost, and high efficiency, uniform dispersion of reactants over the electrode surface is required.²⁸ Traditional flow fields, such as parallel and serpentine flow fields, were employed largely for the anode and cathode flow side.^{29,30} The serpentine flow field has greater reactant distribution and mass transfer capability. In addition, under-rib convection occurs as a result of a pressure variance between two channels.³¹ The serpentine flow field has various disadvantages, including localized flooding and huge pressure drops.³² Vijayakumar *et al.*³³ studied the impact of channel depth (0.2, 0.4, 0.6, 0.8, and 1.0 mm) on a double serpentine flow field with a 45 cm² active area DMFC. They found that while reducing the channel depth from 1 to 0.4 mm, pressure drop increased across the flow field at all current densities and maximum peak power density attained was 47 mW/cm². At higher channel depth, the pressure drop was reduced significantly. At lower channel depth of 0.2 mm, the performance was reduced due to reasons, such as methanol crossover and CO₂ gas void fraction. Oliveira *et al.*³⁴ studied three independent flow channel designs, namely single serpentine flow field (SFF), multi-serpentine flow field (MSFF), and mixed serpentine flow field (MFF) with an L:C ratio of 1.5:2 on a 25 cm² active area DMFC. At higher cell temperature, all the flow fields delivered the same output and, at higher concentration, MSFF delivered better performance. At lower temperature and concentration, all the three flow fields deliver the same performance. At higher concentration, SFF performed well (improvement in cell voltage and power). Ouellette *et al.*³⁵ numerically evaluated the performance of DMFC with changes in the cathode flow field. Parameters, such as input methanol and oxygen concentration, pressure, and velocity, were simulated for serpentine, parallel serpentine, triple serpentine, and grid type flow fields in their numerical studies. The simulation results showed that the grid type flow field delivered the lowest performance due to low dead zones in the cathode. The single serpentine delivered better performance due to better oxidant distribution over the catalyst layer. Lu and Reddy³⁶ studied different flow field designs, namely double channel serpentine flow field (DSFF), single channel serpentine flow field (SSFF), mixed multichannel serpentine with wide channel flow field (MMFW), and mixed multichannel serpentine with narrow channel flow field (MMFN) on DMFC. At a lower flow rate, all flow fields deliver the same performance, but at higher flow rate, MMFW and MMFN performed well. The limitation on 1M methanol concentration was observed as kinetic, ohmic, and mass transport on polarization. While in other concentrations (2–5M), the mass transport limitation disappeared and also increases in methanol flow above 0.1128 ml/min, the performance decreased due to higher pressure drop and methanol crossover. Osman and Ahmed³⁷ studied the impact of anode flow field design to remove the CO₂ bubbles by capillary forces. Hence, they implemented a novel flow field design to enhance the performance at a higher current density. The new design improved performance by 14% and 23% compared to serpentine and parallel flow channels. In the parallel channel, bubble formation was higher and the entire channel was blocked by stagnant slugs. Vasile *et al.*³⁸ conducted numerical investigation on different flow fields (unique serpentine, four parallel serpentine and four inlet serpentine) of DMFC. In that work, they analyzed the mass flow rate, methanol concentration, temperature, anode potential, water and

methanol crossover, current distribution on catalyst layer, and membrane interface to understand the relationship between flow field and cell performance. From the three flow fields, unique serpentine and four inlet serpentine have homogeneous methanol mass fraction and current density distributed on the interface of catalyst layer and membrane. Sachin *et al.*³⁹ investigated several flow field designs, such as single serpentine, double serpentine, and honeycomb. From this study, the honeycomb design had uniform velocity and temperature distribution on the surface of the plate. The honeycomb structure exhibited 11% higher performance than the serpentine flow channel at 3 ml/min.

Rabissi *et al.*⁴⁰ experimentally investigated the performance and durability of scaled up (180 cm² active area) DMFC. From the results, the cell voltage was found degraded about 148 μ V/h over 600 h of test. The issues were mainly caused by dehydration at the cathode inlet and flooding at the outlet. Furthermore, the platinum at the cathode was loaded with parabolic distribution, the performance was improved and the voltage decay was found to be 53.8 μ V/h over 600 h of test. Argyropoulos *et al.*⁴¹ reported that the dynamic characteristic of DMFC was influenced by electrode kinetics and mass transport process, fluid dynamics, and temperature. In a small scale cell (9 cm²), the rate of change of magnitude and load was very quick and reversible. The dynamic response of cell voltage was affected by the methanol flow rate, concentration, and cathode air pressure. On a large scale cell (272 cm²), the cell response was lower than the small scale and its performance was influenced by the anode flow rate and concentration. Scott *et al.*⁴² studied the flow conception of 100 cm² cells to scale up the active area to 225 cm² with parallel flow field, and the author aimed to address important engineering difficulties related to DMFC stack system design and operation. An experimental study on a 200 cm² active area with serpentine flow field discovered that H₂O content increased at the cathode side along the flow channel.⁴³ To scale up a DMFC, single cell with serpentine flow field on the cathode side demands huge pressure drop to remove the condensed water. Hence, to reduce the water flooding, a sinuous flow field was introduced at the cathode.⁴⁴ This finding is important for the current study's flow field selection at the anode and cathode.

On the other hand, the design and functioning of DMFC stacks for various sizes and power outputs were explored. Wang *et al.*⁴⁵ experimentally tested a passive direct methanol fuel cell stack with a 3.5 μ m Au coated on a stainless steel sheet as current collector. It proved that the novel design prevented the electrochemical corrosion and reduced the internal and external connection resistance. From their experimental results, the vertical flow of air in cathode channels delivered better and stable performance (18.7 mW/cm²) than the parallel cathode air channels at 3M methanol concentration. They also investigated the stack for powering a fan for a duration of 100 days. Lee *et al.*⁴⁶ experimentally compared a single cell performance with a stack. The maximum power density achieved by the single cell was 70 mW/cm² at 2M methanol and tested for 3.75 and 250 cc/min of air. The stack delivered 20% higher performance than the single cell, which is attributed to the increased internal temperature compared to that of a single cell. The exothermic reaction made the single cell to reach a temperature of 35 °C; however, in the stack, a highest temperature of 69 °C was recorded. From the results, it was evident that temperature strongly relies on the number of cells and the electric load applied. Masdar *et al.*⁴⁷

investigated an air breathing single cell and a six cell DMFC stack. The power of the stack was 500 mW at 1.5 V in 5M methanol concentration at room temperature. The hexagonal stack with 240 ml reservoir was continuously operated for 40 h. However, in a single cell, 8 ml of 5M methanol reached the same reduction in performance of 25% within 3–4 h. The stack was subjected to 3000 h long term operation after which the Membrane Electrode Assembly (MEA) morphology was analyzed. From their studies, a larger reservoir would be beneficial for long term operations of any electronic device. Further DMFC stacks were designed and evaluated for 33,⁴⁸ 40,⁴⁹ and 50 W⁵⁰ power outputs. A larger DMFC stack (42-cell) with a 138 cm² active area at a maximum power output of 400 W was fabricated and experimented to measure anode and cathode pressure loss for various flow rates.⁵¹ At 0.8 and 0.5M CH₃OH concentrations, the temperature distribution within the cells was uniform. The anode side pressure drops increase with decreasing methanol concentration. The stack was also durability tested for 500 h. The distribution of reactants and internal resistance were the key factors that limited DMFC stack performance.⁵²

The goal of this research is to find the best platinum mass composition on the Pt–NiTiO₃/C anode electrocatalyst and then to implement it on a small scale (25 cm²) DMFC single cell with different flow fields on cathode. The best platinum mass composition and cathode flow field is then further implemented in large scale (100 cm²) DMFC. The resultant performance is compared with the former small scale. Finally, a three-cell stack (3 × 100 cm²) with the similar composition and cathode flow field used in 100 cm² active area is constructed, and the stack's characteristics are tested under numerous running conditions. This is the first ever time to build a multi cell stack utilizing the novel catalyst Pt–NiTiO₃/C with minimum platinum loading of 0.5 mg_{pt}/cm² on 100 cm² active area, which helps to increase the performance in active DMFC.

II. EXPERIMENTAL

A. Materials and synthesis

The anode catalyst material with different mass composition (20%, 40%, 60%) of Pt–NiTiO₃/C, were synthesized by the wet chemical method. The step-by-step procedure for material synthesis is given in Fig. S1. Our earlier article have already included the synthetic techniques and characterization results (x-ray diffraction patterns, TEM images, Selected Area Electron Diffraction (SAED) pattern, cyclic voltammetry, chronoamperometry, XPS analysis, and electrochemical surface area).²⁵ The commercially available carbon cloth (W1S1009) is used as a gas diffusion layer with a microporous layer, Nafion 117, and a cathode catalyst of 0.5 mg_{pt}/cm² with mass composition of 60% Pt and 40% carbon was procured from a Fuel Cell Store in the United States to fabricate the membrane electrode assembly.

B. Catalyst ink preparation and coating

The catalyst ink was prepared by adding 5 wt. % Nafion ionomer and isopropyl alcohol to the catalyst powder. The quantity of Nafion ionomer (0.5 mg/cm²) content for Pt–NiTiO₃/C catalyst was optimized experimentally and published by Kumaresan *et al.*⁵³ After that, the catalyst ink was coated on the Gas Diffusion Layer (GDL) with the help of a bar coater. Using a micropipette, the

catalyst ink was plunged on GDL in front of the blade. The blade helps to spread the catalyst ink until it covers the required area on GDL. The volume of catalyst ink, height of the blade, and speed of drive were modified to obtain the required $0.5 \text{ mg}_{\text{Pt}}/\text{cm}^2$ loading. The coated GDLs were dried for 1 h at 30°C in a nitrogen environment to eliminate remaining oxides from the catalyst surface.

C. Nafion treatment and MEA fabrication

Nafion 117 was pre-treated to increase sulfonic group activity and proton conductivity. Initially, the Nafion membrane was immersed for 1 h in 3% H_2O_2 at 80°C and for 2 h in deionized water. After that, it is immersed in 0.5% H_2SO_4 for an hour. In order to prevent drying, the membrane is cleaned with deionized water. A 25 cm^2 active area gas diffusion electrode (GDE) and a commercial Pt/C GDE were sandwiched together with a Nafion 117 membrane in a hydraulic hot press for 3 min at 130°C .

D. Experimental setup

In this study, the 850e fuel cell test setup (Scribner Associates, USA) was used to evaluate the cell performance using the Fuel Cell 4.3h software. The fuel cell test station can test up to 100 W at 0–20 V and 0–50 A. The anode flow rates were controlled using a peristaltic pump with a maximum flow rate of 480 ml/min. The cathode employed 99.99% pure oxygen as an oxidant, with a maximum flow rate of 1500 ml/min. The cell was heated using the test setup's heater plug and monitored using a K-type thermocouple.

III. RESULTS AND DISCUSSION

A. Mass composition of Pt on performance of DMFC

Initially to find the mass composition of different catalyst powder, the samples were subjected to E-Dax patterns and the results

TABLE I. Electrochemical activity on MOR for various electrode materials.

| Electrode material | Peak current density (mA/cm^2) | References |
|---------------------------------------|--|--------------|
| Pt– CeO_2/C | 80 | 15 |
| Pt– $\text{V}_2\text{O}_5/\text{C}$ | 110 | 16 |
| Pt– Nb_2O_5 | 129 | 57 |
| Pd Al_2O_3 | 39.5 | 58 |
| PtCo/RGO | 38.02 | 59 |
| Pt– MnO_2/RGO | 26 | 60 |
| Pt– NiTiO_3/C (1:1:3) | 98 | 25 |
| Pt– NiTiO_3/C (1:1:3) | 95 | |
| Pt– NiTiO_3/C (2:1:2) | 112 | Present work |
| Pt– NiTiO_3/C (3:1:1) | 114 | |

are shown in Fig. S2 and Table S1. After confirming the mass composition of platinum, the different compositions of catalyst materials were experimented for electrochemical measurements. The experiments are conducted with a conventional three electrode cell system at 25°C . The characterization studies were conducted on 20%, 40%, and 60% Pt on Pt– NiTiO_3/C using biologic test station, and the experiments were conducted on an alkali medium. In cyclic voltammetry, the oxidation peak appeared during the forward scanning and electro-oxidation of methanol occurred during the backward scanning. The experiments were conducted with continuous trails, and the average current density is shown in Fig. 1(a). The average current densities of 20%, 40%, and 60% Pt on Pt– NiTiO_3/C in the alkali medium is 95, 112, and $114 \text{ mA}/\text{cm}^2$, respectively. From the experimental results, 60% Pt delivers better performance than other two combinations. Furthermore, the electrochemical stability was investigated for all the three materials at 0.24 V at room temperature for 1800 s. The results are shown in Fig. 1(b). The present experimental studies are compared with other metal oxide catalysts, and the comparison is given in Table I.

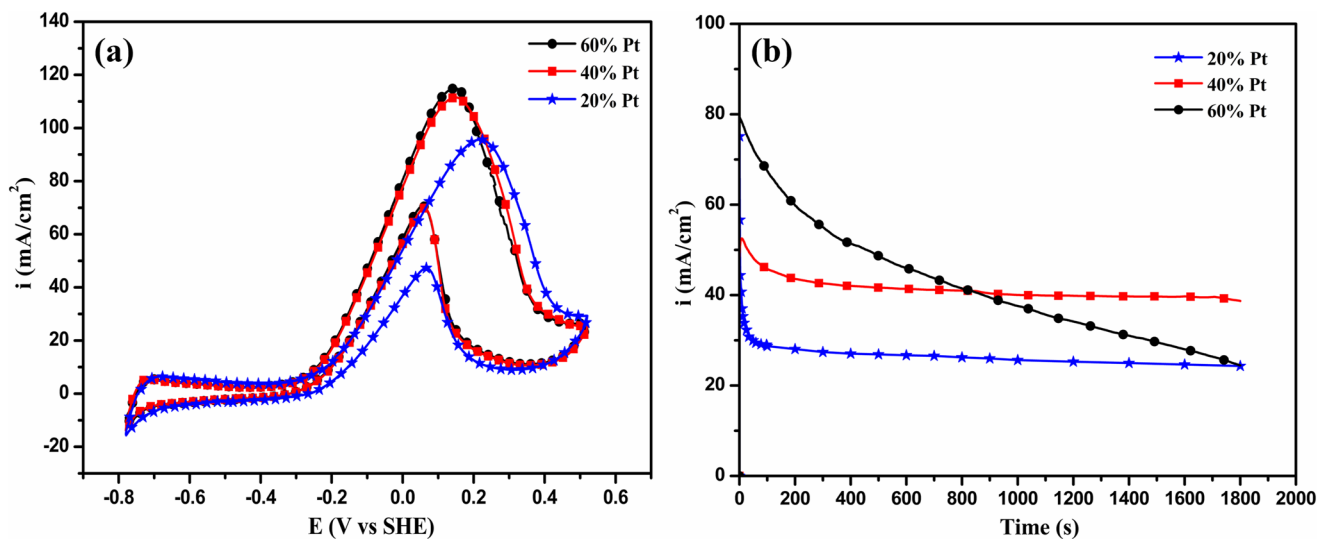


FIG. 1. (a) and (b) CV and CA curves for MOR on the different Pt mass composition on Pt– NiTiO_3/C in 1M $\text{CH}_3\text{OH}/0.5\text{M}$ KOH solution.

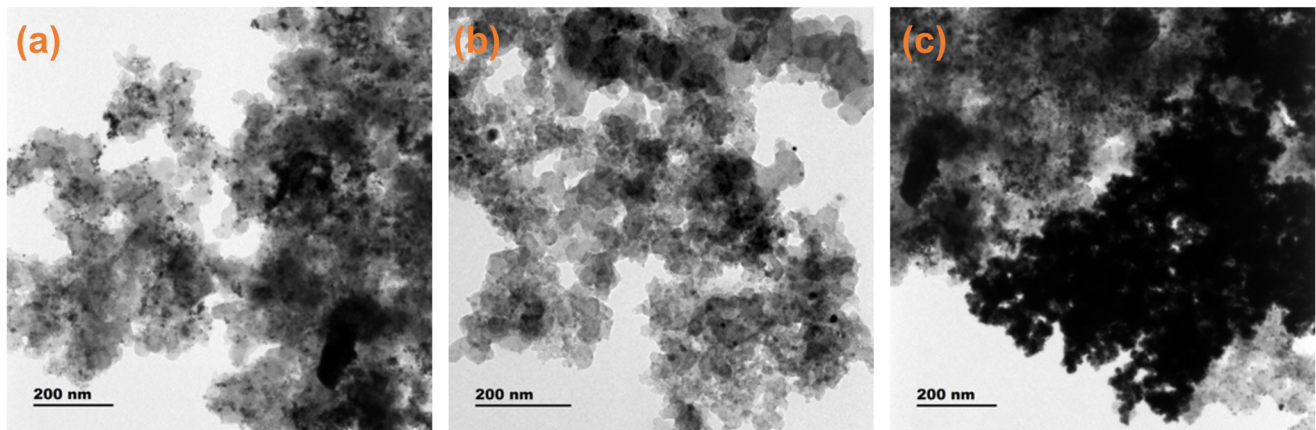
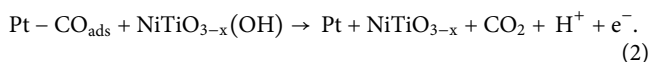
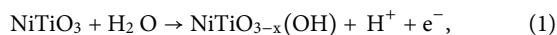


FIG. 2. HRTEM images of Pt-NiTiO₃/C Catalyst with different mass composition of Platinum (a) 20% Pt, (b) 40% Pt, and (c) 60% Pt.

From the stability test, 40% Pt performed well. Initially, 60% Pt starts at higher current and current density declined during the entire period, while for 40% Pt, the current density stabilized at 43 mA/cm², and for 20% Pt, the current density stabilized at 28 mA/cm² at the same potential. From the experimental results, above 40% Pt loading, the methanol electro-oxidation activity decreased for long term operation. This behavior can be attributed to the increased metal load in the catalyst, which could have led to the agglomeration and the subsequent reduction in catalytic active sites.⁵⁴

The agglomeration on the catalyst powder was verified by using TEM images (Fig. 2). The TEM image of 20% Pt on Pt-NiTiO₃/C [Fig. 2(a)] shows even carbon distribution over the surface and identified the metal compounds spread on the carbon surface, while in 40% Pt, the metal compounds were distributed evenly with some agglomeration, which can be clearly seen in Fig. 2(b). Meanwhile, in 60% Pt, the materials were completely agglomerated, which can be visualized in Fig. 2(c). From the electrochemical studies, the mass composition of Pt-NiTiO₃/C catalyst powder was approximated. Additionally, NiTiO₃ harbors the capacity to absorb OH⁻ (active oxygen) from the aqueous electrolyte and deliver to Pt for the conversion of CO species.^{55,56} Thus, the bi-functional mechanism was proposed by the following reactions:



After completing the electrochemical studies, the catalyst material was coated on the GDL using a bar coater. In order to evaluate the consequence of different platinum mass compositions (20%, 40%, and 60%) on the Pt-NiTiO₃/C electrocatalyst, three membrane electrode assemblies were fabricated. The performance analysis was conducted with all three different MEAs at their operating conditions given in Table II.

The MEAs were prepared with 20%, 40%, and 60% platinum composition in the electrocatalyst, and performance analysis was

conducted. The results are shown in Fig. 3(a). After completing the conditioning of the MEA, polarization curves were drawn by reducing the voltage from 0.6 to 0.1 V at an interval of 0.05 V. From the experiment, the maximum performance delivered by the 20% Pt composition was 17.86 mW/cm². At 40%, Pt-NiTiO₃/C cell was seen to deliver a 26.9% improvement in maximum power density compared to 20% Pt-NiTiO₃/C. This is partly due to the increase in mass composition of platinum, reducing the catalyst layer thickness for the same catalyst stuffing.²⁷ Hence, it is proved that while reducing the thickness of the catalyst layer, the performance increased proportionally. The maximum number of Pt-NiTiO₃ dual active sites on the surface of the catalyst contributes to its high catalytic activity.²⁶

Further increasing platinum composition to 60% showed a 10.4% reduction in maximum power compared to the 40% platinum composition. In 60% Pt, the metal compound in the catalyst powder

TABLE II. Operating parameters of DMFC with 25 cm².

| | Parameters | Values |
|---------|---------------------|---------------------------------------|
| Anode | Reactant | Methanol |
| | Concentration | 1.0M |
| | Flow rate | 3 ml/min |
| | Catalyst | Pt-NiTiO ₃ /C |
| | Loading of platinum | 0.5 mg _{pt} /cm ² |
| | Flow field | Serpentine (L:C 2 × 2) |
| Cathode | Reactant | Oxygen (99.99) |
| | Flow rate | 100 ml/min |
| | Humidity | 100% RH |
| | Catalyst | Pt/C |
| | Loading | 0.5 mg _{pt} /cm ² |
| | Flow field | Serpentine (L:C 2 × 2) |
| Others | Cell temperature | 80 °C |

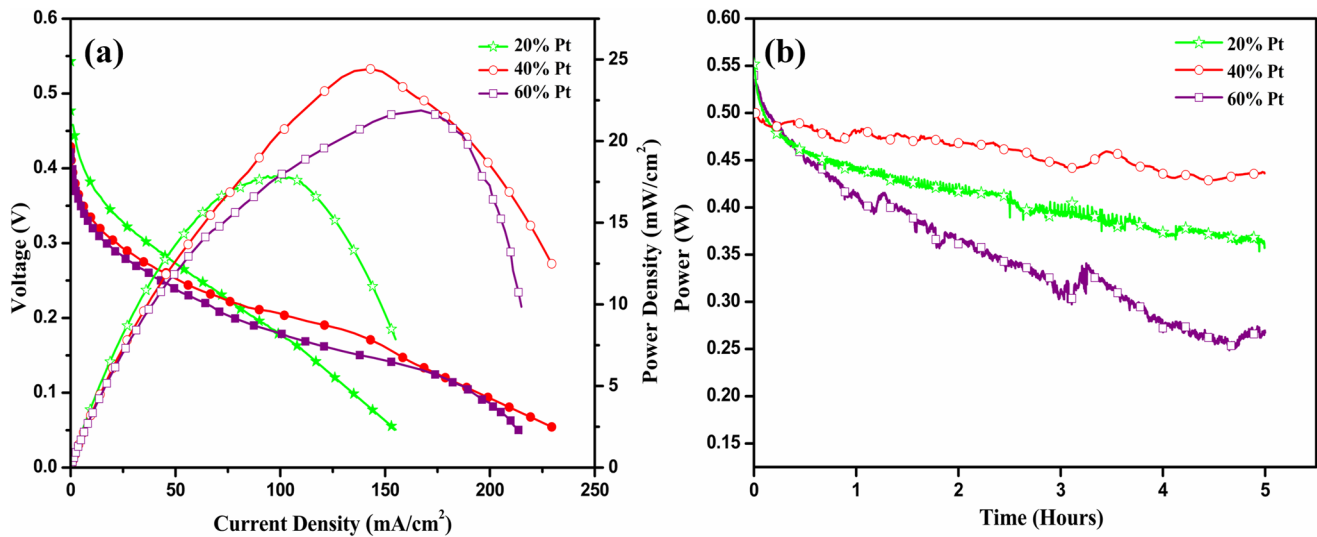


FIG. 3. (a) Polarization and Power Density curves (b) Durability of DMFCs based on different mass composition 20%, 40%, and 60% Pt on Pt–NiTiO₃/C with 25 cm² active area.

was higher. Because of that, the catalyst powder was likely not properly bonded to the GDL during the MEA fabrication. From this, the activity of the catalyst was lower in lower mass composition and it is mostly due to the lesser number of double active areas on the catalyst surface. Even if a catalyst with a greater platinum mass composition has more dual active sites on the catalyst surface, the decrease in catalyst activity is primarily attributable to bigger particle size due to increased metal stuffing.⁶¹ The particle size was evaluated from TEM images using Image J software, and the average size of 20% Pt, 40% Pt, and 60% Pt on Pt–NiTiO₃/C is 6.5, 6.9, and 7.1 nm, respectively. The maximum power was reached at 0.17 V, which is due to the particle size of the catalyst. Platinum particle size is a key factor, which influences the cell potential. While increasing the Pt particle size, the cell potential will be reduced. The cell sacrifices its voltage at higher current to deliver maximum power, which was experimentally studied by Shan *et al.*¹⁴ Despite having a smaller surface area than XC-72, the catalyst can disperse Pt–NiTiO₃ well at 20% and 40% stuffing. With 60% Pt stuffing, the catalyst had poor Pt–NiTiO₃ dispersion due to very low carbon content (20%), and the results are shown in Fig. 2.

Further the stability of three different catalyst mass compositions, durability tests were conducted. The results are shown in Fig. 3(b). From the results, it is confirmed that the 40% Pt–NiTiO₃/C delivered stable performance at a constant voltage of 0.16 V. The fluctuations were observed in the result, during the top up of methanol fuel, insufficient diffusion of methanol at starting stage,⁶² flooding (Cathode water formation),⁶³ methanol crossover,⁶⁴ reduction in oxygen reduction reaction at the cathode side,⁶⁵ CO formation at the anode,⁶⁶ and also the maximum power extraction from the cell for long term operations. At the same voltage, 20% of platinum was also tested. It delivers lower performance than 40% of platinum. The depth of the gas diffusion layer was measured to be 368 μm (GDL from Fuel Cell Store). The gas diffusion electrode

thickness of 20%, 40%, and 60% Pt was measured to be 451, 424, and 394 μm, respectively. The thickness was measured from SEM images after completing all the experiments, and the images are shown in Fig. 4.

By increasing the thickness of the GDE, the performance was reduced due to the increase in ohmic resistance and ion transfer resistance. At a lower catalyst layer thickness, the maximum penetration depth is also lower, which results in enhancement of reactant distribution and subsequent products to the catalyst sites.⁶⁷ Thus, it is apparent that the catalyst layer thickness plays a vital role in fuel cells. With 60% of platinum, the power output at the initial stage was better than in the other two compositions, and the performance was reduced drastically in further processes. It is due to the higher metal composition available in the catalyst (80% of metals). Due to low carbon content, the metal was not bounded properly on the catalyst layer; hence, leaching of catalyst from GDL was clearly visible in the outlet of anode along with methanol solution. The catalytic sites are active partially for electrochemical reaction at greater stuffing, resulting in poor utilization and only slight improvements in cell performance.⁶⁸

B. Post-exsitu analysis Pt–NiTiO₃/C MEA

The SEM analysis of the best performing MEA with 40% Pt–NiTiO₃/C catalyst is shown in Fig. 5 after performance analysis and 5 h of continuous operation for durability. Figure 5(a) shows the cross-sectional view of MEA. Catalyst layer's elemental mappings are shown in Figs. 5(b)–5(g) corresponding to the elements, such as carbon, oxygen, nickel, platinum, titanium, and overall top view of MEA with Pt–NiTiO₃/C catalyst, respectively. The distribution of catalysts on the catalyst layer is uniform, as shown in Fig. 5(g). From this study, the uniform distribution of the catalyst on the active sites has been observed, which ensures that the leach out of the catalyst on

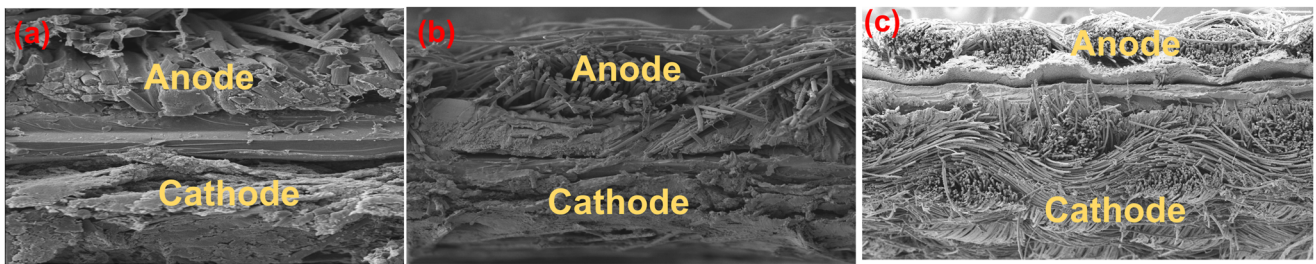


FIG. 4. MEA of PtNiTiO₃/C with different anode platinum mass composition (a) 20% Pt, (b) 40% Pt, and (c) 60% Pt.

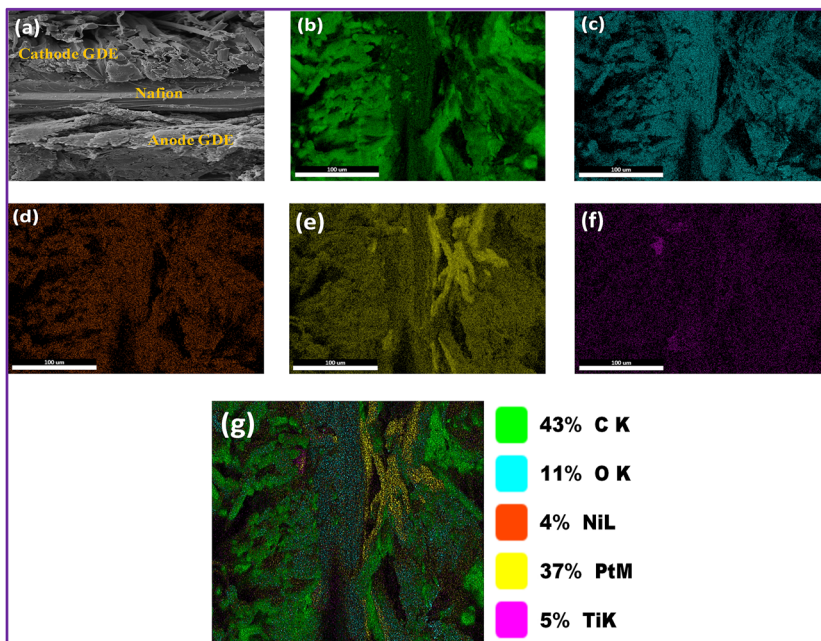


FIG. 5. SEM results of (a) cross-sectional view of MEA along with elemental mapping (b) Carbon, (c) Oxygen, (d) Nickel, (e) Platinum, (f) Titanium, (g) top view Pt-NiTiO₃/C catalyst coated.

carbon has drastically diminished. The GDE (anode) was found to have a thickness of 426 μm . The chemical composition of the unique Pt-NiTiO₃/C catalyst found in GDE is shown in Fig. 5(g).

C. State of art comparison with commercial catalyst

The best performing MEA had a mass composition of 40% Pt, 20% NiTiO₃, and 40% C, and it was tested and compared to a commercial MEA with the same mass composition. The commercial MEA with 0.5 $\text{mg}_{\text{Pt}}/\text{cm}^2$ catalyst, which contains 40% Pt, 20% Ru, and 40% C as anode catalysts and 60% Pt and 40% C as cathode catalysts, was purchased from Fuel Cell Store in the United States. The results clearly demonstrate that the commercial MEAs will deliver 21.53 mW/cm^2 at 0.18 V, which is in accordance with the specifications, and the experimental results are shown in Fig. 6. The performance was 12% lower than our novel catalyst material, which demonstrates that the novel catalyst material outperformed

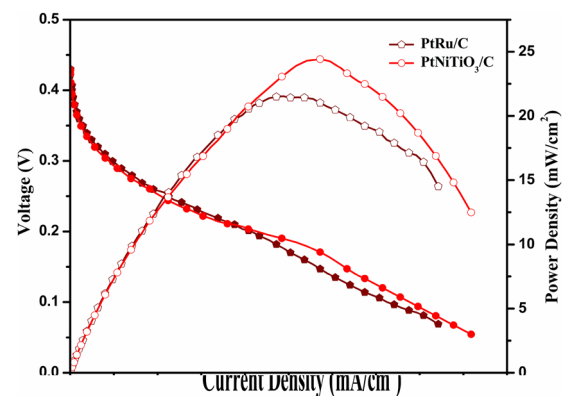


FIG. 6. Polarization and Power Density curves of DMFCs based on 40% Pt on Pt-NiTiO₃/C and Pt-Ru/C with 25 cm^2 active area.

TABLE III. Performance of different platinum mass composition in a 25 cm² active area.

| Sl. No. | Catalyst | | Loading | Mass composition | Membrane | Commercial/ home made | Peak power density (mW/cm ²) |
|---------|-------------------------|---------|---------------------------------------|--------------------------------------|------------|--------------------------|---|
| | Anode | Cathode | | | | | |
| 1 | PtNiTiO ₃ /C | | 0.5 mg _{pt} /cm ² | 20% Pt–20% NiTiO ₃ –60% C | Nafion 117 | Home made | 17.86 |
| 2 | PtNiTiO ₃ /C | | | 40% Pt–20% NiTiO ₃ –40% C | | | |
| 3 | PtNiTiO ₃ /C | Pt/C | | 60% Pt–20% NiTiO ₃ –20% C | | | |
| 4 | PtRu/C | | | 40% Pt–20% Ru–40% C | | | |

the commercial MEA. From these experiments, it was proved that the NiTiO₃ supportive material aids in the conversion of CO to CO₂ species better than the commercial Ru material. The maximum power obtained in the commercial MEA with Pt–Ru/C catalyst and the homemade MEAs with Pt–NiTiO₃/C catalyst was listed in Table III.

D. Effect of cathode flow field design on performance of DMFC

From the above experiments, the best performing catalyst powder mass composition was taken and applied to different cathode flow fields (serpentine, parallel, and sinuous). Yang and Zhao⁶⁹ and Dohle *et al.*⁷⁰ found that a reactant in the flow field is dispersed more uniformly when the channel to width ratio and number of channels are increased, resulting in increased fuel consumption. In addition, based on our former studies, the rib and channel width were set as 2 × 2 mm² for all flow fields.⁷¹ The sinuous flow field was numerically investigated on DMFC by Ramasamy *et al.*⁷² who proved that the flow field has better water removal capability at the cathode. The flow field designs taken for the present study are shown in Fig. 7.

In that research, the influence of pressure drops, velocity, oxygen concentration, and water formation was studied numerically. The cathode flow field was altered in all three trials to evacuate water production. To minimize flooding, the cathode flow channel area must be large enough to disperse oxygen throughout the GDL. The serpentine flow field is also the best flow field for anode⁷³ due to its longer channels and higher pressure drop; the reactants are dispersed evenly throughout the GDL.^{69,74} The oxygen concentration discrepancies among the channel and the under-land zones is another key challenge at the cathode.⁷⁵ Cathode flow-field designs impact mass transfer of oxygen and water drainage. Flooding

happens if the created water is not rapidly evacuated. The DMFCs performance with various flow field configurations can be evaluated in this context. The performance analysis was conducted with all three cathode flow field arrangements with the similar operating conditions given in Table II. The performance analysis for the different flow fields is shown in Fig. 8(a), and the data are compiled in Table IV.

Initially, a serpentine flow field was utilized for both the anode and cathode and the maximum performance obtained was 24.42 mW/cm² at 0.17 V. The resistance on the wall and channel bend causes a larger pressure reduction in serpentine flow fields. This allows O₂ to react properly, resulting in better diffusion and even spreading of O₂ to the GDL. However, a larger pressure drop demands more energy.⁵³ After that, the cathode flow field was changed to a parallel flow field, and it delivers a maximum performance of 18.65 mW/cm², which is 23% less than the serpentine flow field. It is evident that parallel channels are inferior in mass transport.

From the above two experiments, to optimize the pressure drop, reaction rate, and flow of reactants toward the GDL, the serpentine and parallel flow fields were combined. The parallel flow field was modified by providing bends on the straight channels and it was named as sinuous flow field. Manso *et al.*⁷⁶ made a review on major revelations concerning under rib convection and sub-rib convection, stating that this spectacle is prominent in channel curves and improves Proton Exchange Membrane Fuel Cell (PEMFC) power. The numerical and experimental studies were conducted on PEMFCs using the sinuous flow field at the anode and cathode by Vijayakrishnan *et al.*⁴⁴ From the studies, it is proved that the sinuous cathode flow field helps to increase the performance by 17%. Hence, an identical sinuous flow field was used at the cathode end in the current study because the Oxygen Reduction Reaction (ORR) in the cathode on PEMFCs and DMFCs was similar.

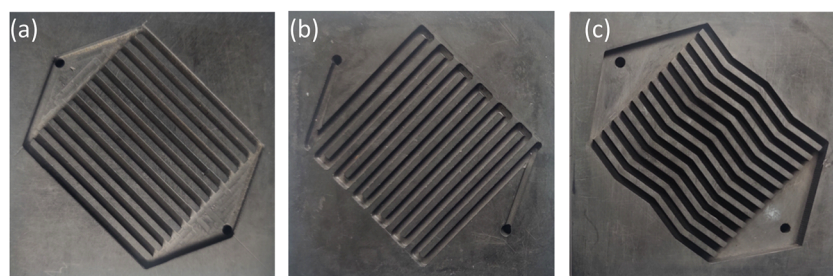


FIG. 7. Different flow field designs for 25 cm² active area DMFC (a) Serpentine (b) Parallel (c) Sinuous.

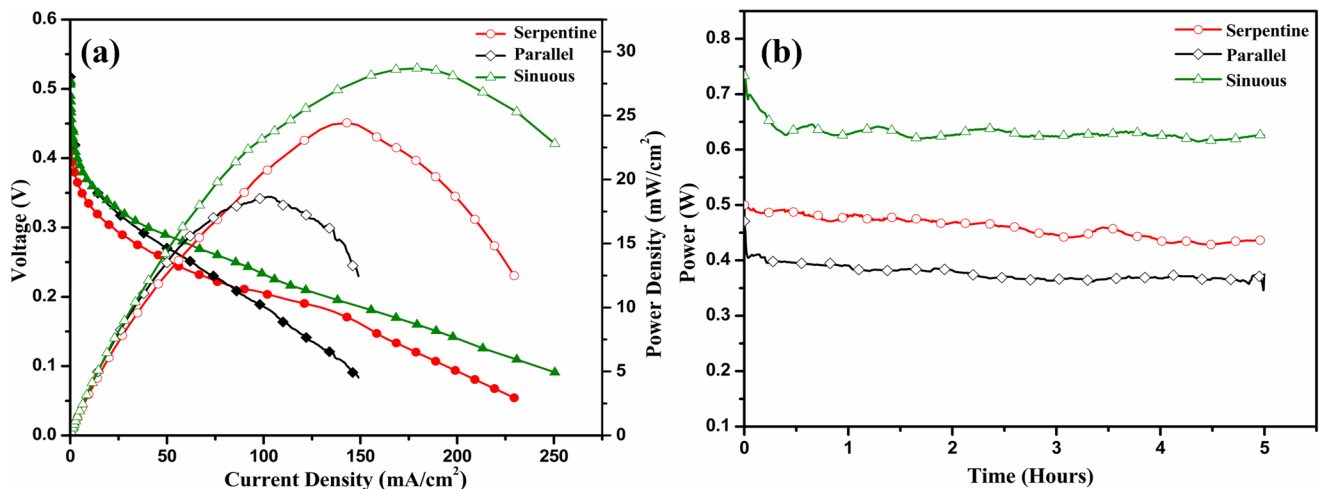


FIG. 8. (a) Polarization and Power Density curves (b) Durability of DMFC based on different cathode flow field configuration.

TABLE IV. Performance of various cathode flow fields in a 25 cm² active area.

| Present work | Catalyst (0.5 mg _{Pt} cm ⁻²) | | Flow fields (L:C ratio 2 × 2 mm ²) | | Voltage (V) | Max. power density (mW/cm ²) |
|--------------|---|---------------|--|------------|-------------|--|
| | Anode | Cathode | Anode | Cathode | | |
| | PtNiTiO ₃ /C (40% Pt) | Pt/C (60% Pt) | Serpentine | Serpentine | 0.17 | 24.42 |
| | | | Serpentine | Parallel | 0.16 | 18.65 |
| | | | | Sinuous | 0.16 | 28.69 |

Hence, using the sinuous flow field, experiments were conducted on a 25 cm² DMFC. The experimental results proved that the novel flow field delivered better performance with a maximum performance of 28.69 mW/cm² at 0.16 V. It is 15% higher in performance than the serpentine flow field and 35% higher in performance than the parallel flow channel. The increment in performance was due to the flow of reactants toward the GDL and also because the distance between the inlet and outlet of the flow field was kept very low and it helps to remove water formed inside the channel. In the sinuous flow field, owing to higher reduction in pressure diffusion, high convection in the crosswise direction better performance was achieved. At cathode, it leads to reduction in performance due to water lodging, which was eliminated in the sinuous flow field.

To find the cell stability with different flow fields, a short time durability analysis was carried out with different flow field configurations. All the experiments were conducted at the same flow rate and temperature, which was used for performance analysis. The experiments were conducted with a constant voltage process, the voltage was fixed at 0.17 V for all three experiments, and results are given in Fig. 8(b). The serpentine flow field delivered a stable performance from 0.5 to 0.45 W; only 0.05 W power deviation during the durability studies was found. While conducting continuous experiments, the water formed inside the cathode channel was not effectively removed from the flow field. Hence, the performance

decreased slowly. Using the parallel flow channel, durability studies were conducted with the same voltage and the initial voltage was lesser than the serpentine flow field. The deviations in parallel flow channel were 15% from the initial to the end of the experiments. However, in the serpentine flow design, it is only a 10% deviation. Finally, the sinuous flow field was tested for durability. The results were more stable than the other two results. The performance was also higher, and the deviation during durability was only 6%. This is owing to the collective outcome of serpentine and parallel flow channel configurations. As a result, the flow-field configuration of the cathode has the greatest influence on DMFC performance and stability.

E. Performance of scaled up DMFC

The performance of a scaled-up DMFC with serpentine and sinuous flow fields as the anode and cathode, with the same land to channel ratio followed in a 25 cm² active area, was examined in more detail. The flow channel with an active area of 100 cm² DMFCs anode and cathode is shown in Figs. 9(a) and 9(b). Compared to the 25 cm² sinuous flow field, the 100 cm² sinuous flow field has two inlets on the cathode side. Maldistribution of the reactants flow is one of the key problems in scaling up of DMFC.²⁸ Hence, design modification is needed for uniform velocity distribution with two

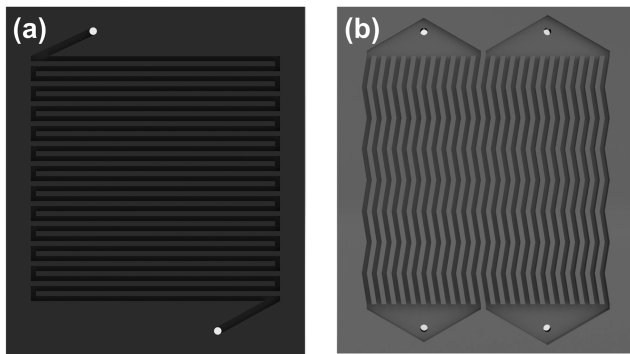


FIG. 9. Flow fields of 100 cm² active area DMFC (a) Anode (Serpentine) (b) Cathode (Sinuous).

inlets and two outlets were compared by Magesh Kannan.⁷⁷ The flow was homogeneously distributed when there are higher than 13 flow channels with one inlet at flow rates up to 0.5 l/min¹. Thus, in this investigation, the cathode side flow field is separated into pieces of no more than 13 channels. For each segment, the enlarged sinuous flow field contains two inlets and exits.

Two flat plate heaters were placed on either side of the cell in order to evenly distribute the temperature throughout the cell. Following the achievement of the cell temperature, the experiments were conducted with a large scale DMFC and the results were compared with those obtained with a 25 cm² DMFC in order to determine the performance difference between 25 and 100 cm². The performance analysis was conducted with the same operating conditions given in Table II, the cathode flow field was fixed with sinuous, and the cathode flow rate was 500 ml/min.

At a voltage of 0.16 V, the peak power density obtained in large scale DMFCs was 23.82 mW/cm², which is shown in

Fig. 10(a). This represents a 17% reduction in power density compared to the 25 cm² active area, which is attributed to higher electric, ionic, and mass transport loss of components. Furthermore, the reactants were propelled by pressure-assisted flow (PAF). By increasing the cell active area from 25 to 100 cm², the ohmic resistance was increased.⁴⁴ This will increase the ohmic losses. Both ohmic and concentration losses contribute to reduced performance of the 100 cm² active area DMFC. Longer channels caused considerable pressure drop between the inlet and outlet, resulting in high parasitic energy needs.⁷⁸ CO₂ bubble removal inside the anode flow channel is also a contributing factor to cell performance degradation.

After completing the performance analysis on the large-scale DMFC, the MEA was subjected to a durability test in order to determine its longevity. At 0.2 V for a total of 5 h, the voltage was maintained at this level during the durability testing process. The long-term performance of a larger-scale DMFC with a novel flow field was evaluated in this test. According to the results in Fig. 10(b), a large number of fluctuations were found, but fluctuations in fuel cells at low voltages are relatively common due to the two-phase liquid-gas interaction in the flow fields at higher current densities. Initially, the power was 1.4 W, and it was eventually reduced to 1.36 W. In this case, the deviation was only 3%. As a result of the durability results, our novel flow field was found to be suitable for larger-scale fuel cells that produce a stable and improved power output.

F. Performance analysis of 5 W DMFC stack

Based on the results of the single cell, a DMFC stack with a graphite plate three cell stack was manufactured with the serpentine and sinuous flow field designs machined. A three-cell stack was assembled using two bipolar plates and two unipolar plates along with their MEAs, current collector plates, insulators, and the aluminum end plates.

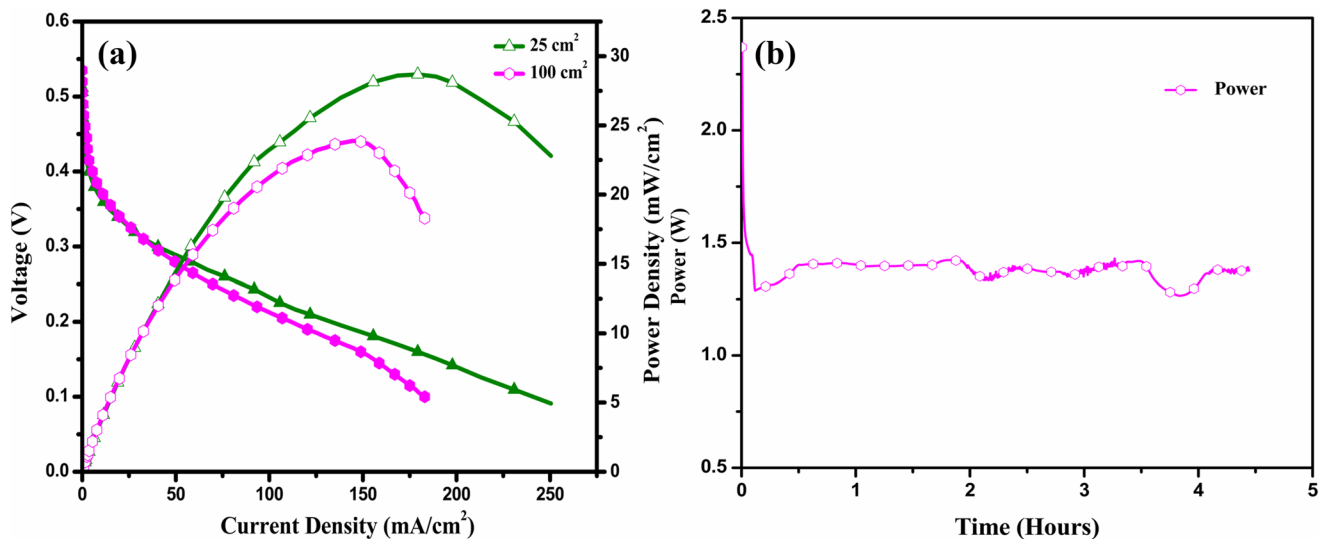


FIG. 10. (a) Polarization and Power Density curves (b) Durability of scaled up DMFC with 100 cm² active area.

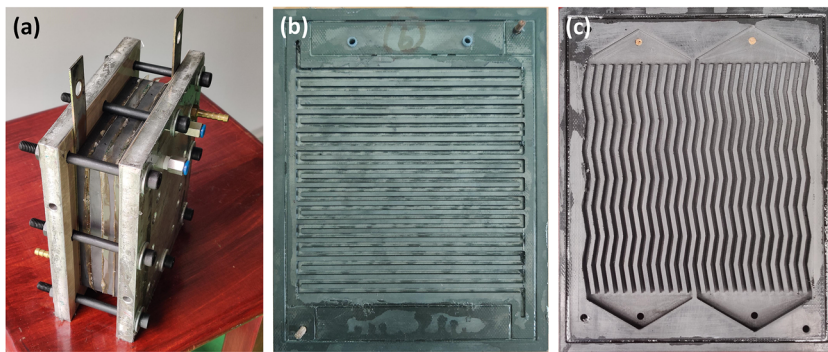


FIG. 11. (a) Three cell stack ($3 \times 100 \text{ cm}^2$) (b) serpentine (c) sinuous.

TABLE V. Operating parameters of DMFC with a 100 cm^2 active area three-cell stack.

| Parameters | | Values |
|------------|----------------------|-----------------------|
| Anode | Flow rate | 3, 5, 7, and 9 ml/min |
| | Flow field (bipolar) | Serpentine |
| Cathode | Flow rate | 500 ml/min |
| | Flow field (bipolar) | Sinuous |

The images of DMFC stack and the flow field used in the anode and cathode are shown in Fig. 11. A reliable stack and comparable performance to single cells is difficult to achieve due to glitches, such as leakage and intermixing of reactants, nonuniform reactant distribution throughout the cell, and the deviation in the activity of MEAs used in the stack. Hence, a simple flow analysis was conducted with cathode flow fields assembled with three cells in series, and the results are shown in Fig. S3.

The graphic depicts the assembled view of a three-cell stack with an active area of 100 cm^2 per cell. Following the completion of the assembling procedure, the stack was first subjected to a leak test to determine its integrity. Deionized water was used throughout the anode flow field to verify the presence of leaks. After the leakage test, the reactants (methanol solution and pure oxygen) were delivered into the anode and cathode sides of the stack in a counter flow arrangement. The operating parameters of three cell stack are shown in Table V.

Figure 12(a) depicts the performance of the stack at various methanol flow rates with 1M methanol concentration. With single cells, the highest performance was obtained at a flow rate of 3 ml min^{-1} and a total power output of 2.4 W. The best anode reactant flow rate for a DMFC stack was determined by varying it from 3 to 9 ml/min with an interval of 2 ml/min. The flow rate appeared to be proportional to the number of unit cells, but it was not. The best results were obtained at a 5 ml/min flow rate, 5.64 W maximum power at 0.7 V voltage. The maximum flow rate was then increased up to 9 ml/min. The higher the fluid pressure, the more likely the

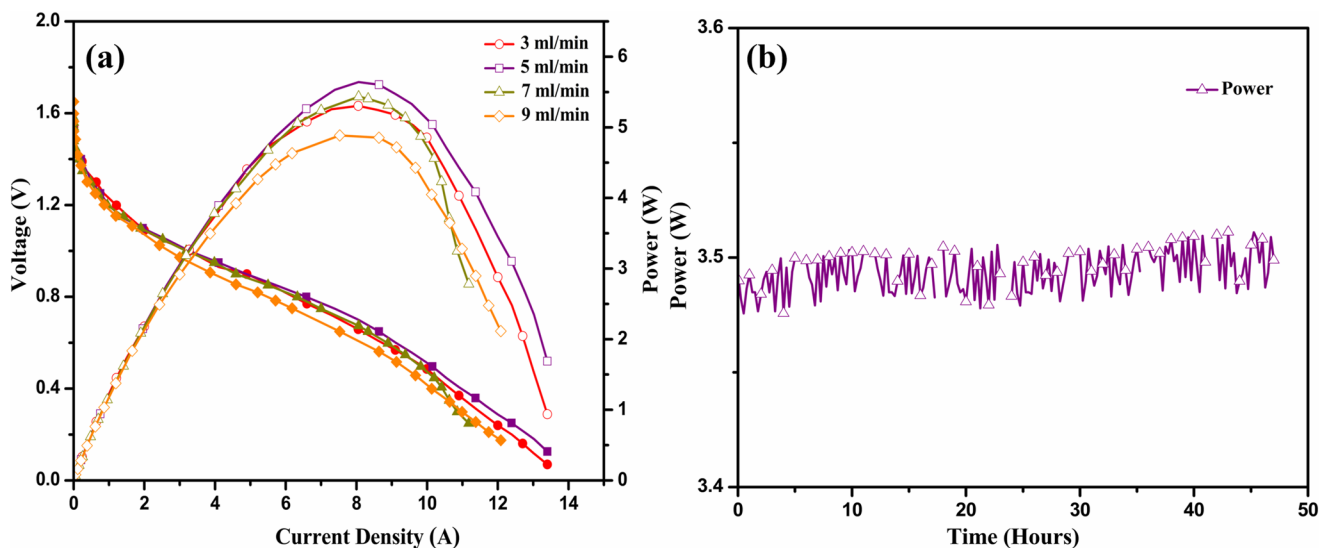


FIG. 12. (a) Polarization and Power Density curves off stack with different methanol flow rates (b) Durability of scaled up DMFC stack ($3 \times 100 \text{ cm}^2$).

stack will leak. Also, at a lower flow rate, some cells in the stack will be unused because they can operate at higher current densities than the imposed.⁷⁹ It is possible that this is owing to the increased rate of methanol crossover at higher flow rates due to a higher pressure drop, which reduces cell performance by generating a mixed potential at the cathode.

A durability test was then carried out for 48 h with an optimal flow rate on the stack. Figure 12(b) depicts the outcomes of the study. The voltage for the stack was kept constant at 0.8 V throughout the experiment. Increased spikes in the durability graph were observed, and this is due to the addition of fuel to the fuel tank. The test station is turned off every 5 h in order to keep the circuit temperature constant due to laboratory operations. In addition, the cell's performance returned to normal after being shut off after 5 h of operation and then resumed after an hour of inactivity. From Fig. 5, repeated shutdowns and operations may cause this issue. Because of electro-osmotic drag and concentration gradient, there may be a water build-up on the cathode side, which had diffused from the anode. There may also be an accumulation of CO₂ created by electrochemical methanol oxidation in the anode, which could explain the brief deactivation.

IV. CONCLUSIONS

This research investigates the experimental analysis of DMFCs based on Pt–NiTiO₃/C anode catalysts, including platinum compositions of 20, 40, and 60 wt. %. It was found that the best-performing DMFC composition was identical to that of the standard Pt–Ru/C catalyst DMFC. Following the experiments, best mass composition was used with different cathode flow fields (serpentine, parallel, and sinuous) and the large-scale DMFC with the best flow field configurations was tested while operating at a constant temperature of 80 °C. Different anode flow rates (3, 5, 7, and 9 ml/min) were then tested to see how they affect the performance of the DMFC three cell stack. The key conclusions from the experiments are listed as follows:

- The electrochemical and physicochemical characterizations for various anode mass compositions of Pt–NiTiO₃/C have been studied.
- The DMFCs based on Pt–NiTiO₃/C anode electrocatalysts containing 40 wt. %, of Pt yielded 26.8% and 10.4% more power density in comparison to 20 and 60 wt. % anode electrocatalysts. Hence, 40 wt. % of Pt is the most stable for DMFC.
- The sinuous flow channel promotes uniform gas distribution and reduces pressure loss; they have the potential to increase fuel cell performance over standard designs.
- The power density of DMFCs with sinuous cathode flow fields was 17.48% and 53.83% higher than that of DMFCs with serpentine and parallel cathode flow fields.
- In comparison to DMFCs with a 25 cm² active area, the power density of DMFCs with a 100 cm² active area was 17% lower due to ohmic resistance, concentration loss and by-product effect.
- Pt–NiTiO₃/C and sinuous cathode flow field DMFC stack (3 × 100 cm²) provide maximum power of 5.64 W at 5 ml/min. From these studies, it is proved that the flow rate provided to a single cell was not suitable for stack operations.

- From the stack durability operation, it is proved that the DMFC stack with Pt–NiTiO₃/C catalyst and sinuous flow field is best suitable for DMFC applications.

SUPPLEMENTARY MATERIAL

See the [supplementary material](#) that includes the E-Dax analysis of different Pt mass composition, x-ray diffraction pattern, and x-ray photoelectron spectroscopy of PtNiTiO₃/C catalyst material and cathode flow distribution analysis of three cell stack with novel flow field.

ACKNOWLEDGMENTS

We gratefully acknowledge DST-UKIERI (Grant No. DST/INT/UK/P121/2016), India, and Loughborough University, UK, for the financial support. The support and facilities provided by the PSG management are acknowledged.

AUTHOR DECLARATIONS

Conflict of Interest

The authors have no conflicts to disclose.

Author Contributions

Thanarajan Kumaresan: Data curation (lead); Formal analysis (lead); Methodology (equal); Writing – original draft (lead). **Karthikeyan Palaniswamy:** Funding acquisition (lead); Supervision (lead); Writing – review & editing (equal). **Ashley Fly:** Project administration (equal); Writing – review & editing (equal). **Senthilarasu Sundaram:** Supervision (equal); Writing – review & editing (equal).

DATA AVAILABILITY

The data that support the findings of this study are available from the corresponding author upon reasonable request.

REFERENCES

- ¹Y. Bicer and I. Dincer, *Int. J. Hydrogen Energy* **42**, 3767 (2017).
- ²S. Changizian, P. Ahmadi, M. Raeesi, and N. Javani, *Int. J. Hydrogen Energy* **45**, 35180 (2020).
- ³K. Priya, K. Sathishkumar, and N. Rajasekar, *Renewable Sustainable Energy Rev.* **93**, 121 (2018).
- ⁴J. Pandey and A. Shukla, *Solid State Ionics* **262**, 811 (2014).
- ⁵M. Goor, S. Menkin, and E. Peled, *Int. J. Hydrogen Energy* **44**, 3138 (2019).
- ⁶M. U. Karaođlan, A. C. İnce, C. O. Colpan, A. Glösen, N. S. Kuralay, M. Müller, and D. Stolten, *Int. J. Hydrogen Energy* **44**, 18981 (2019).
- ⁷X. Li and A. Faghri, *J. Power Sources* **226**, 223 (2013).
- ⁸S. Basri, S. K. Kamarudin, W. R. W. Daud, and Z. Yaakub, *Int. J. Hydrogen Energy* **35**, 7957 (2010).
- ⁹S. Wang, G. Sun, G. Wang, Z. Zhou, X. Zhao, H. Sun, X. Fan, B. Yi, and Q. Xin, *Electrochem. Commun.* **7**, 1007 (2005).
- ¹⁰Y. M. Alyousef, M. K. Datta, S. C. Yao, and P. N. Kumta, *J. Phys. Chem. Solids* **70**, 1019 (2009).
- ¹¹P. Justin and G. Ranga Rao, *Int. J. Hydrogen Energy* **36**, 5875 (2011).
- ¹²Y. Zhang, H. Zhang, Y. Ma, J. Cheng, H. Zhong, S. Song, and H. Ma, *J. Power Sources* **195**, 142 (2010).

- ¹³M. Ercelik, A. Ozden, E. Seker, and C. O. Colpan, *Int. J. Hydrogen Energy* **42**, 21518 (2017).
- ¹⁴C.-C. Shan, D.-S. Tsai, Y.-S. Huang, S.-H. Jian, and C.-L. Cheng, *Chem. Mater.* **19**, 424 (2007).
- ¹⁵M. A. Scibioh, S.-K. Kim, E. A. Cho, T.-H. Lim, S.-A. Hong, and H. Y. Ha, *Appl. Catal., B* **84**, 773 (2008).
- ¹⁶T. Maiyalagan and F. N. Khan, *Catal. Commun.* **10**, 433 (2009).
- ¹⁷J. M. Macak, P. J. Barczuk, H. Tsuchiya, M. Z. Nowakowska, A. Ghicov, M. Chojak, S. Bauer, S. Virtanen, P. J. Kulesza, and P. Schmuki, *Electrochem. Commun.* **7**, 1417 (2005).
- ¹⁸R. E. Fuentes, B. L. García, and J. W. Weidner, *J. Electrochem. Soc.* **158**, B461 (2011).
- ¹⁹P. Xiao, X. Guo, D.-J. Guo, H.-Q. Song, J. Sun, Z. Lv, Y. Liu, X.-P. Qiu, W.-T. Zhu, L.-Q. Chen, and U. Stimming, *Electrochim. Acta* **58**, 541 (2011).
- ²⁰H.-J. Kim, D.-Y. Kim, H. Han, and Y.-G. Shul, *J. Power Sources* **159**, 484 (2006).
- ²¹K. Drew, G. Girishkumar, K. Vinodgopal, and P. V. Kamat, *J. Phys. Chem. B* **109**, 11851 (2005).
- ²²S. L. Gojković, B. M. Babić, V. R. Radmilović, and N. V. Krstajić, *J. Electroanal. Chem.* **639**, 161 (2010).
- ²³X. Zhao, J. Zhu, L. Liang, J. Liao, C. Liu, and W. Xing, *J. Mater. Chem.* **22**, 19718 (2012).
- ²⁴T. Ioroi, Z. Siroma, N. Fujiwara, S.-i. Yamazaki, and K. Yasuda, *Electrochem. Commun.* **7**, 183 (2005).
- ²⁵V. Thiagarajan, R. Manoharan, P. Karthikeyan, E. Nikhila, A. Hernández-Ramírez, and F. J. Rodríguez-Varela, *Int. J. Hydrogen Energy* **42**, 9795 (2017).
- ²⁶V. Thiagarajan, P. Karthikeyan, K. Thanarajan, S. Neelakrishnan, R. Manoharan, R. Chen, A. Fly, R. Anand, T. R. Karuppa Raj, and N. Sendhil Kumar, *Int. J. Hydrogen Energy* **44**, 13415 (2019).
- ²⁷Z. D. Wei, H. B. Ran, X. A. Liu, Y. Liu, C. X. Sun, S. H. Chan, and P. K. Shen, *Electrochim. Acta* **51**, 3091 (2006).
- ²⁸M. Mortada, H. S. Ramadan, J. Faraj, A. Faraj, H. El Hage, and M. Khaled, *Int. J. Hydrogen Energy* **46**, 32161 (2021).
- ²⁹D. H. Jeon, S. Greenway, S. Shimpalee, and J. W. Van Zee, *Int. J. Hydrogen Energy* **33**, 1052 (2008).
- ³⁰J. Bachman, A. Santamaria, H.-Y. Tang, and J. W. Park, *J. Power Sources* **198**, 143 (2012).
- ³¹K.-S. Choi, H.-M. Kim, and S.-M. Moon, *Int. J. Hydrogen Energy* **36**, 1613 (2011).
- ³²J. P. Kloess, X. Wang, J. Liu, Z. Shi, and L. Guessous, *J. Power Sources* **188**, 132 (2009).
- ³³R. Vijayakumar, M. Rajkumar, P. Sridhar, and S. Pitchumani, *J. Appl. Electrochem.* **42**, 319 (2012).
- ³⁴V. B. Oliveira, C. M. Rangel, and A. M. F. R. Pinto, *Chem. Eng. J.* **157**, 174 (2010).
- ³⁵D. Ouellette, U. Gencalp, and C. O. Colpan, *Int. J. Hydrogen Energy* **42**, 2680 (2017).
- ³⁶Y. Lu and R. G. Reddy, *Int. J. Hydrogen Energy* **36**, 822 (2011).
- ³⁷S. Osman and M. Ahmed, *Energy Convers. Manage.* **251**, 114958 (2022).
- ³⁸N. S. Vasile, A. H. A. Monteverde Videla, C. Simari, I. Nicotera, and S. Specchia, *Int. J. Hydrogen Energy* **42**, 27995 (2017).
- ³⁹P. V. Sachin, A. Sathish, and T. S. Boopathi, *J. Phys.: Conf. Ser.* **2070**, 012081 (2021).
- ⁴⁰C. Rabissi, M. Zago, L. Grahl-Madsen, M. Odgaard, and A. Casalegno, *J. Power Sources* **506**, 230218 (2021).
- ⁴¹P. Argyropoulos, W. M. Taama, and K. Scott, "Engineering & modelling of large scale liquid FED direct methanol fuel cells stacks," in *Institution of Chemical Engineers Symposium Series* (U.S. Environmental Protection Agency, 1999), pp. 21–30.
- ⁴²K. Scott, W. M. Taama, and P. Argyropoulos, *J. Power Sources* **79**, 43 (1999).
- ⁴³N. S. M. Hassan, W. R. W. Daud, K. Sopian, and J. Sahari, *J. Power Sources* **193**, 249 (2009).
- ⁴⁴M. K. Vijaykrishnan, K. Palaniswamy, J. Ramasamy, T. Kumaresan, K. Manoharan, T. K. Raj Rajagopal, T. Maiyalagan, V. R. Jothi, and S.-C. Yi, *Int. J. Hydrogen Energy* **45**, 7848 (2020).
- ⁴⁵L. Wang, Z. Yuan, F. Wen, Y. Cheng, Y. Zhang, and G. Wang, *Energy* **144**, 587 (2018).
- ⁴⁶S. Lee, D. Kim, J. Lee, S. T. Chung, and H. Y. Ha, *Korean J. Chem. Eng.* **22**, 406 (2005).
- ⁴⁷M. S. Masdar, Dedikarni, A. M. Zainoodin, M. I. Rosli, S. K. Kamarudin, and W. R. W. Daud, *Int. J. Hydrogen Energy* **42**, 9230 (2017).
- ⁴⁸C. Y. Chen, J. Y. Shiu, and Y. S. Lee, *J. Power Sources* **159**, 1042 (2006).
- ⁴⁹A. Manokaran, R. Vijayakumar, T. N. Thomman, P. Sridhar, S. Pitchumani, and A. K. Shukla, *J. Chem. Sci.* **123**, 343 (2011).
- ⁵⁰D. Kim, J. Lee, T.-H. Lim, I.-H. Oh, and H. Y. Ha, *J. Power Sources* **155**, 203 (2006).
- ⁵¹H. Dohle, H. Schmitz, T. Bewer, J. Mergel, and D. Stolten, *J. Power Sources* **106**, 313 (2002).
- ⁵²D. Buttin, M. Dupont, M. Straumann, R. Gille, J.-C. Dubois, R. Ornelas, G. P. Fleba, E. Ramunni, V. Antonucci, A. S. Aricò, P. Cretì, E. Modica, M. Pham-Thi, and J.-P. Ganne, *J. Appl. Electrochem.* **31**, 275 (2001).
- ⁵³T. Kumaresan, T. Velumani, M. Chandran, K. Palaniswamy, A. Thirkell, A. Fly, R. Chen, and S. Sundaram, *Mater. Lett.* **276**, 128222 (2020).
- ⁵⁴A. Caglar, T. Sahan, M. S. Cogenli, A. B. Yurtcan, N. Aktas, and H. Kivrak, *Int. J. Hydrogen Energy* **43**, 11002 (2018).
- ⁵⁵R. Mancharan and J. B. Goodenough, *J. Mater. Chem.* **2**, 875 (1992).
- ⁵⁶R. Manoharan and J. Prabhuram, *J. Power Sources* **96**, 220 (2001).
- ⁵⁷P. Justin, P. H. K. Charan, and G. R. Rao, *Appl. Catal., B* **100**, 510 (2010).
- ⁵⁸W.-L. Qu, Z.-B. Wang, Z.-Z. Jiang, D.-M. Gu, and G.-P. Yin, *RSC Adv.* **2**, 344 (2012).
- ⁵⁹R. Baronia, J. Goel, S. Tiwari, P. Singh, D. Singh, S. P. Singh, and S. K. Singhal, *Int. J. Hydrogen Energy* **42**, 10238 (2017).
- ⁶⁰W. Yuan, Y. Zhang, N. Zhang, C. Yin, X. Zhang, and X. Liu, *Catal. Commun.* **100**, 66 (2017).
- ⁶¹M. Y. Lo, I. Liao, and C. Huang, *Int. J. Hydrogen Energy* **32**, 731 (2007).
- ⁶²C. Y. Chen and C. Tsao, *Int. J. Hydrogen Energy* **31**, 391 (2006).
- ⁶³H. S. Casalongue, S. Kaya, V. Viswanathan, D. J. Miller, D. Friebe, H. A. Hansen, J. K. Nørskov, A. Nilsson, and H. Ogasawara, *Nat. Commun.* **4**, 2817 (2013).
- ⁶⁴S. Sharma and B. G. Pollet, *J. Power Sources* **208**, 96 (2012).
- ⁶⁵K. Matsuoka, Y. Iriyama, T. Abe, M. Matsuoka, and Z. Ogumi, *Electrochim. Acta* **51**, 1085 (2005).
- ⁶⁶G.-B. Jung, A. Su, C.-H. Tu, and F.-B. Weng, *J. Fuel Cell Sci. Technol.* **2**, 81 (2005).
- ⁶⁷D. E. Glass, G. A. Olah, and G. K. S. Prakash, *J. Power Sources* **352**, 165 (2017).
- ⁶⁸A. Havránek and K. Wippermann, *J. Electroanal. Chem.* **567**, 305 (2004).
- ⁶⁹H. Yang and T. S. Zhao, *Electrochim. Acta* **50**, 3243 (2005).
- ⁷⁰H. Dohle, A. A. Kornyshev, A. A. Kulikovskiy, J. Mergel, and D. Stolten, *Electrochem. Commun.* **3**, 73 (2001).
- ⁷¹K. Thanarajan, V. Magesh Kannan, M. Karthikeyan, V. Thiagarajan, R. Manoharan, and P. Karthikeyan, "Consequence of rib width and channel width on performance of 70CM2 PEMFC," *Int. J. Automob. Eng. Res. Dev.* **39–46** (2017).
- ⁷²J. Ramasamy, K. Palaniswamy, T. Kumaresan, M. Chandran, and R. Chen, *Int. J. Hydrogen Energy* **47**, 595 (2022).
- ⁷³D. Ouellette, A. Ozden, M. Ercelik, C. O. Colpan, H. Ganjehsarabi, X. Li, and F. Hamdullahpur, *Int. J. Hydrogen Energy* **43**, 1152 (2018).
- ⁷⁴M. Marappan, K. Palaniswamy, T. Velumani, K. B. Chul, R. Velayutham, P. Shivakumar, and S. Sundaram, *Chem. Rec.* **21**, 663 (2021).
- ⁷⁵T. S. Zhao, C. Xu, R. Chen, and W. W. Yang, *Prog. Energy Combust. Sci.* **35**, 275 (2009).
- ⁷⁶A. P. Manso, F. F. Marzo, J. Barranco, X. Garikano, and M. Garmendia Mujika, *Int. J. Hydrogen Energy* **37**, 15256 (2012).
- ⁷⁷V. Magesh Kannan, Design and development of high performance scaled up PEM fuel cell by flow channel modifications, Anna University, 2020.
- ⁷⁸G.-B. Jung, A. Su, C.-H. Tu, Y.-T. Lin, F.-B. Weng, and S.-H. Chan, *J. Power Sources* **171**, 212 (2007).
- ⁷⁹H. Liu and P. Li, *Int. J. Hydrogen Energy* **38**, 3757 (2013).